Springer

Journal of
Mechanical
Science and
Technology

Journal of Mechanical Science and Technology 23 (2009) 2891~2902

www.springerlink.com/content/1738-494x
DOI 10.1007/s12206-009-0805-6

Probabilistic modeling of stress-based FLD in tube hydroforming process †

Jeong Kim[1,*], Woo-Jin Song[2] and Beom-Soo Kang[3]

[1]*Department of Aerospace Engineering, Pusan National University, Busan, 609-735, Korea*
[2]*Industrial Liaison Innovation Centerr, Pusan National University, Busan, 609-735, Korea*
[3]*ERC/NSDM, Pusan National University, Busan, 609-735, Korea*

(Manuscript Received November 10, 2008; Revised July 11, 2009; Accepted July 28, 2009)

Abstract

Recently a stress-based FLD due to its path-independency has become a new mainstream technology for prediction of forming limit in tube hydroforming processes, which usually have non-linear strain path. However, the random characteristics owing to experimental errors, inherent measuring equipment errors, dimensional tolerance of as-received blank, inconsistent lubrication condition and so on lead to uncertainty with regard to the position of the forming limit curve on the stress-based FLD. In this work, to take into account the uncertainty on the stress-based FLD, a probabilistic modeling on the stress-based FLD with confidence level is firstly attempted. With the assumption of all experimentally measured data as normally distributed random variables, stochastic evaluation of the reliability of the stress-based FLD is carried out. Moreover the statistical correlation between measured data during a bulge test and the material parameters is investigated by using the first-order approximated mean value and variance. The reliability is analytically calculated based on first-order reliability method (FORM) and verified with Monte-Carlo simulation (MCS). Finally, at a given deviation of measured data, the band width of forming limit curve on the stress-based FLD to be able to satisfy the required confidence level is determined.

Keywords: Hydroforming; Stress-based FLD; Probabilistic modeling; Reliability; First-order reliability method (FORM); Monte-Carlo simulation (MCS)

1. Introduction

In general, a frequently used technique for evaluating busting failure in sheet metal forming is the forming limit diagram (FLD), where principal strain pairs are compared to a forming limit curve (FLC). In practice, a scatter band rather than a curve is obtained. The classical FLD method has been proven to be useful in judging forming severity in industry. However, the strain path dependency of the FLD is obviously a serious limitation to its use whenever non-proportional strain paths, especially as in hydroforming processes, are expected. One way to overcome this disadvantage is to use a forming limit stress diagram (FLSD). As the more general forming limit criterion, it was found that a stress-based forming limit criterion was independent of the strain path and then adopted the criterion for analysis of flanging dies [1]. Afterward, the effect of FLSD was rediscovered and it was necessary to use the FLSD in all forming processes [2, 3]. Furthermore, the calculation of stress-based forming limits based on experimental strain data using the method proposed by Stoughton and a more relevant study on the application of stress-based forming limit criterion under linear and complex strain paths were performed [4]. To predict the onset of necking in sheet metal loaded under non-proportional load paths, as well as under three-

† This paper was recommended for publication in revised form by Associate Editor Tae Hee Lee

*Corresponding author. Tel.: +82 51 510 2477, Fax.: +82 51 513 3760
E-mail address: greatkj@pusan.ac.kr

dimensional stress states, an extended stress-based forming limit curve (XSFLC) was proposed [5].

Although there are many experimental and theoretical studies to predict the forming limits, it is crucial to recognize that the use of FLD or FLSD has definite limitations. First, there are different variations in the experiment procedure and material parameters that lead to uncertainties in the evaluation of the stress-based FLD for a given process. In other words, the variability of the raw material parameters such as strength coefficient, work hardening, anisotropy, yield stress and so on causes uncertainty with regard to the position of the forming limit curve on the stress-based FLD. In addition, the measured data naturally has random characteristics due to experimental errors, inherent measuring equipment errors, dimensional tolerance of as-received tube, inconsistent lubrication condition and so on. Taking the variation of the material parameters into account, several researchers [6-8] have proposed a more general concept, namely the forming limit band (FLB), as a region covering the entire dispersion of the forming limit curves in Fig. 1. The strain-based forming limit curve for reliability analysis combined with the sheet forming simulation and the system reliability assessment techniques was established [9]. These works in the literature pointed out that the location of the forming limit curve with some uncertainties should be dealt with. Though few research works attempted to study the effect of the material parameters on the dispersion of strain-based forming limit curve, a systematic and practical approach to figure out the reliability of the stress-based forming limit curve due to variation of the material parameters was rare.

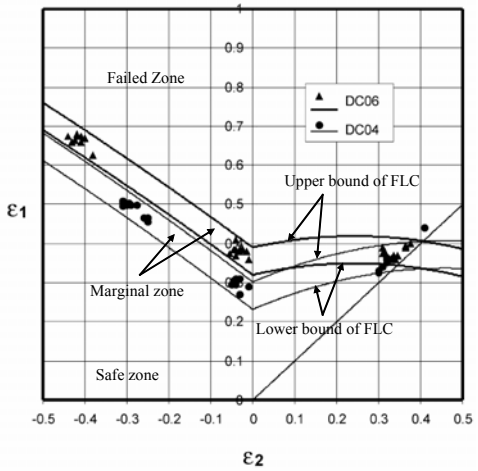

Fig. 1. A forming limit band in a strain-based FLD [8].

In this paper, firstly, in order to theoretically construct the deterministic stress-based FLD, plastic instability based on the Hill's quadratic plastic potential is introduced. Since the theoretical limit stress on the FLSD is a function of the only strength coefficient, work-hardening exponent and anisotropy parameter, accurate and appropriate material properties of tubular material need to be measured under the actual condition in hydroforming. Thus the statistical correlation between the material parameters and measured data during a bulge test is evaluated by using the first-order approximate mean value and variance. All experimentally measured data are assumed as normally distributed random variables to take into account the uncertainty in the material parameters. And then, a stochastic modeling on the stress-based FLC with confidence level is first attempted and statistical evaluation of the reliability of the stress-based FLD is carried out. The reliability was analytically calculated based on first-order reliability method(FORM) and verified with Monte-Carlo simulation(MCS). Finally, at a given deviation of material parameters, the bandwidth of the forming limit curve on the stress-based FLD is determined to be able to satisfy the required confidence level.

2. Analytical determination of stress-based FLD

2.1 Plastic instability based on diffuse necking

Consider a tube to be thin enough for the plane stress hypothesis to be valid. From Hill's quadratic yield criterion for anisotropic materials [10],

$$2f(\sigma_{ij}) = F(\sigma_y - \sigma_z)^2 + G(\sigma_z - \sigma_x)^2 + H(\sigma_x - \sigma_y)^2 + 2L\tau_{yz}^2 + 2M\tau_{zx}^2 + 2N\tau_{xy}^2 = 1 \quad (1)$$

where *F, G, H, L, M*, and *N* are the anisotropy parameters. And *f* is the plastic potential identified as the scalar function that defines the elastic limit surface. Then under plane stress condition, the effective stress for planar isotropic materials can be written as follows:

$$\bar{\sigma} = \sqrt{\sigma_1^2 + \sigma_2^2 - \frac{2R}{R+1}\sigma_1\sigma_2} \quad (2)$$

where σ_1 and σ_2 are the principal hoop and axial stress, *R* is an anisotropy parameter. The plastic strain increments are given by considering the normality

condition, incompressibility condition and the equivalent work definition of effective strain increment as follows:

$$\begin{aligned} d\bar{\varepsilon} &= \frac{1+R}{\sqrt{1+2R}}\sqrt{d\varepsilon_1^{\,2}+d\varepsilon_2^{\,2}+\frac{2R}{R+1}d\varepsilon_1 d\varepsilon_2} \\ d\varepsilon_1 &= \frac{d\bar{\varepsilon}}{\bar{\sigma}}\left[\sigma_1-\frac{R}{1+R}\sigma_2\right] \\ d\varepsilon_2 &= \frac{d\bar{\varepsilon}}{\bar{\sigma}}\left[\sigma_2-\frac{R}{1+R}\sigma_1\right] \\ d\varepsilon_3 &= -\left(d\varepsilon_1+d\varepsilon_2\right) \end{aligned} \tag{3}$$

where $d\varepsilon_1$, $d\varepsilon_2$ and $d\varepsilon_3$ are the plastic strain incremental components along the principal hoop, axial and thickness directions, respectively.

Assuming that principal stresses maintain constant ratios and directions, the ratio of stresses and strain increments also will not change as represented by $\alpha=\sigma_2/\sigma_1$, $\beta=d\varepsilon_2/d\varepsilon_1$. From the diffuse necking criterion, the condition for plastic instability is satisfied when the load reaches a maximum value along both principal directions as,

$$d(P+\pi r^2 p)=0 \quad \& \quad d(prl)=0 \tag{4}$$

where p is an internal hydraulic pressure and P is an axial force, which are applied independently. Also r and l are the current values of the radius and length of the tube. This condition leads to the following simultaneous constraints: $d\sigma_1=\sigma_1 d\varepsilon_1$ and $d\sigma_2=\sigma_2 d\varepsilon_2$. Thus the following instability criterion in terms of sub-tangent Z for the anisotropic materials can be obtained as [11],

$$\frac{1}{Z}=\frac{1}{\bar{\sigma}}\frac{d\bar{\sigma}}{d\bar{\varepsilon}}\le\frac{\alpha(2\alpha-\rho)^2+(2-\alpha\rho)^2}{4(1-\alpha\rho+\alpha^2)^{3/2}}\equiv\frac{\boldsymbol{\Psi}}{\boldsymbol{\Omega}} \tag{5}$$

where $\rho=2R/(1+R)$.

2.2 Limit stresses for stress-based FLC

To obtain forming limit curves in terms of limit stresses, it is necessary to introduce critical principal strains ε_1^c, ε_2^c along the hoop and axial direction, respectively. With the work-hardening law $\bar{\sigma}=K\bar{\varepsilon}^n$, Eq. (5) can be written as

$$\frac{1}{Z}=\frac{1}{\bar{\sigma}}\frac{d\bar{\sigma}}{d\bar{\varepsilon}}=\frac{n}{\bar{\varepsilon}}=\frac{\boldsymbol{\Psi}}{\boldsymbol{\Omega}} \tag{6}$$

Assuming proportional loading, the equivalent strain can be described as

$$\bar{\varepsilon}=\frac{1+R}{\sqrt{1+2R}}\sqrt{\varepsilon_1^{\,2}+\varepsilon_2^{\,2}+\frac{2R}{R+1}\varepsilon_1\varepsilon_2}=\boldsymbol{\Theta}\varepsilon_1 \tag{7}$$

where $\boldsymbol{\Theta}=(1+R)\left(1+\beta\rho+\beta^2\right)^{0.5}(1+2R)^{-0.5}$.

According to Eqs. (6) and (7), the limit strains based on the plasticity instability yield as

$$\begin{aligned} \varepsilon_1^c &= \frac{\boldsymbol{\Omega} n}{\boldsymbol{\Theta}\boldsymbol{\Psi}} \\ \varepsilon_2^c &= \beta\varepsilon_1^c \end{aligned} \tag{8}$$

In addition, the plastic strain components along the principal hoop and axial directions from Eq. (3) can be also expressed in terms of limit strain and stress components

$$\begin{aligned} \varepsilon_1^c &= \frac{\bar{\varepsilon}}{\bar{\sigma}}\left[\sigma_1^c-\frac{R}{1+R}\sigma_2^c\right] \\ \varepsilon_2^c &= \frac{\bar{\varepsilon}}{\bar{\sigma}}\left[\sigma_2^c-\frac{R}{1+R}\sigma_1^c\right] \end{aligned} \tag{9}$$

Finally, the limit hoop and axial stress, σ_1^c and σ_2^c, when the bursting failure occurs, can be obtained as

$$\begin{aligned} \sigma_1^c &= \frac{(1+R)^2}{1+2R}\frac{\bar{\sigma}}{\bar{\varepsilon}}\left[\varepsilon_1^c+\frac{R}{1+R}\varepsilon_2^c\right] \\ \sigma_2^c &= \frac{(1+R)^2}{1+2R}\frac{\bar{\sigma}}{\bar{\varepsilon}}\left[\varepsilon_2^c+\frac{R}{1+R}\varepsilon_1^c\right] \end{aligned} \tag{10}$$

3. Stochastic material parameters

Above all, in order to analytically construct the stress-based FLD in terms of limit stresses in Eq. (9), the limit strains should be calculated according to specific strain ratios from Eq. (8). Since the limit strain is a function of the material parameter n and R, accurate and appropriate material properties of tubular material need to be measured under the actual condition in hydroforming. Thus the following data should be measured during bulging of tubes to analytically predict limit strains and stresses as shown in Fig. 2(a) radius of curvature in hoop direction ρ_1, (b) radius of curvature in longitudinal direction ρ_2, (c) internal pressure p, (d) thickness t, (e) friction coefficient μ and (f) axial feeding force P_a. These measurements are converted into true stress–strain data

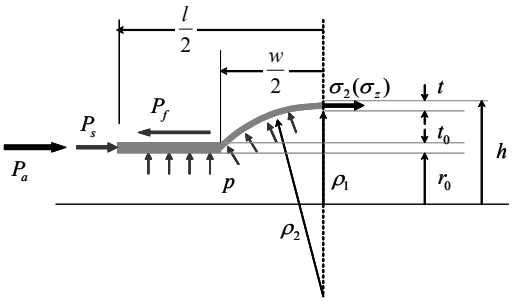

Fig. 2. Free body diagram for free bulge test of tubular blank.

through an analytical procedure, and then the flow stress characteristics of the tubular material are obtained from fitting into known and accepted forms, finally as will be mentioned in Section 3.1.

3.1 Flow stress obtained from tube bulging

Consider a thin-walled, open-end tube under internal hydraulic pressure and axial load, which are applied independently. The finite strain components for *i*th different bulging stage can be calculated from the measured data as the following equations:

$$\varepsilon_1^i = \ln\left(\frac{\rho_1^i}{\rho_0}\right), \varepsilon_3^i = \ln\left(\frac{t^i}{t_0}\right)$$
$$\varepsilon_2^i = -\left(\varepsilon_1^i + \varepsilon_3^i\right) = \ln\left(\frac{l^i}{l_0}\right) \tag{11}$$

where ρ_0, t_0 and l_0 are the initial inner radius, wall thickness and length of the tube, respectively. The tube in the die cavity is assumed to be thin enough for the plane stress hypothesis to be valid. For an element at bulging tip of the tube, the following equilibrium equation can be written [12]:

$$\frac{\sigma_1^i}{\rho_1^i} + \frac{\sigma_2^i}{\rho_2^i} = \frac{p^i}{t^i} \tag{12}$$

The two radii of curvature ρ_1 and ρ_2 can be calculated with the measured bulge height *h* in Fig. 2:

$$\rho_1 = \frac{h}{2} \tag{13}$$

$$\rho_2 = \frac{w^2 + h^2 - 4h\rho_0 + 4\rho_0^2}{4(h - 2\rho_0)} \tag{14}$$

The force equilibrium in axial direction of tubular blank, which is exerted in the bulged tube, can be expressed as follows:

$$\sigma_2^i\left[2\pi\rho_1^i t^i\right] = p^i\pi\left(\rho_1^i\right)^2 + P_f^i - P_a^i - P_s^i \tag{15}$$

where P_f^i, P_s^i and P_a^i are the friction force between tool and tube, sealing force against pressurized fluid, and the force to feed the tube in axial direction for *i*th different pressure level, respectively. As can be seen in Eq. (15), the frictional effect between free bulge die and tubular blank was considered in this work, and the axial force to seal the tubular blank against pressurizing was also taken into account to derive the force equilibrium to accurately describe the actual test condition. These forces induced by frictional effect and tube sealing can be expressed as Eqs. (16) and (17).

$$P_f^i = \mu\left[p^i\left(2\pi\rho_0\right)\left(\frac{l^i - w}{2}\right)\right] = \mu p^i\pi\rho_0\left(l_0 e^{\varepsilon_2^i} - w\right) \tag{16}$$

$$P_s^i = p^i\pi\rho_0^2 \tag{17}$$

where μ means the friction coefficient, *w* is bulge width and l^i is tube length for *i*th different bulging stage, respectively. Once stress and strain components are calculated, effective stress $\bar{\sigma}^i$ and effect strain $\bar{\varepsilon}^i$ for *i*th pressure level can be determined from Eqs. (2) and (3). More frequently, the anisotropic parameter *R* in Eq. (2) for normal anisotropy materials is represented by the quantities r_0, r_{45} and r_{90},

$$R = \frac{r_0 + 2r_{45} + r_{90}}{4} \tag{18}$$

where 0, 45 and 90 refer to the angle made with the rolling direction. Finally, successive effective stress and effective strain values can be fitted into the general power law as the following.

$$\bar{\sigma} = K\bar{\varepsilon}^n \tag{19}$$

Using the least square method, the strength coefficient *K* and work-hardening exponent *n* can be deduced by

$$\ln K = \frac{\sum_{j=1}^{q} \ln\bar{\sigma}^j}{q} \tag{20}$$

$$n = \frac{\sum_{j=1}^{q}\left[\ln\bar{\varepsilon}^{j} - E\left(\ln\bar{\varepsilon}\right)\right]\left[\ln\bar{\sigma}^{j} - E\left(\ln\bar{\sigma}\right)\right]}{\sum_{j=1}^{q}\left[\ln\bar{\varepsilon}^{j} - E\left(\ln\bar{\varepsilon}\right)\right]^{2}} \quad (21)$$

where q is total number of bulging stages and $E(\mathbf{Z})$ denotes mean value of a random variable $\mathbf{Z}$.

3.2 Variances of material parameters

Since the measured data naturally have random characteristics due to experimental errors, inherent measuring equipment errors, dimensional tolerance of as-received tube, inconsistent lubrication condition and so on, the internal pressure p, thickness t, bulge height h, friction coefficient μ, and three anisotropy parameters r_0, r_{45} and r_{90} can be considered as normally distributed random variables. Namely, a random vector $\mathbf{Z} = \left[p^i, \cdots, p^q, t^i, \cdots, t^q, h^i, \cdots, h^q, \mu\right]^T$.

Since the limit stress is a function of only material parameter K, n and R, the statistical correlation between the material parameters and measured data needs to be evaluated. For a general function of several random variables, $G(\mathbf{Z})$, the first-order approximate mean value, denoted as $E[\ldots]$, and variance, denoted as $Var[\ldots]$ of $G(\mathbf{Z})$ are as follows [13]:

$$E[G(\mathbf{Z})] = G(\mathbf{Z})\big|_{E[\mathbf{z}]} \quad (22)$$

$$Var[G(\mathbf{Z})] \equiv \sigma_G^2 = \sum_{j=1}^{m}\left(\left.\frac{\partial G}{\partial Z_j}\right|_{E[\mathbf{Z}]}\right)^2 \sigma_{Z_j}^2 \quad (23)$$

Thus, with the assumption of all random variables to be statistically independent, the mean value and variance of K can be determined by

$$E[K(\mathbf{Z})] \equiv \bar{K} = K(\mathbf{Z})\big|_{E[\mathbf{Z}]} \quad (24)$$

$$\begin{aligned} Var[K(\mathbf{Z})] &\equiv \sigma_K^2 \\ &= \sum_{j=1}^{q}\left(\left.\frac{\partial K}{\partial p^j}\right|_{E[\mathbf{Z}]}\right)^2 \sigma_p^2 + \sum_{j=1}^{q}\left(\left.\frac{\partial K}{\partial t^j}\right|_{E[\mathbf{Z}]}\right)^2 \sigma_t^2 \\ &+ \sum_{j=1}^{q}\left(\left.\frac{\partial K}{\partial h^j}\right|_{E[\mathbf{Z}]}\right)^2 \sigma_h^2 + \left(\left.\frac{\partial K}{\partial \mu^j}\right|_{E[\mathbf{Z}]}\right)^2 \sigma_\mu^2 \end{aligned} \quad (25)$$

In a similar way, the mean values and variances of n and R can be obtained from

$$E[n(\mathbf{Z})] \equiv \bar{n} = n(\mathbf{Z})\big|_{E[\mathbf{Z}]} \quad (26)$$

$$E[R(\mathbf{Z})] \equiv \bar{R} = R(\mathbf{Z})\big|_{E[\mathbf{Z}]} \quad (27)$$

$$\begin{aligned} Var[n(\mathbf{Z})] &\equiv \sigma_n^2 \\ &= \sum_{j=1}^{q}\left(\left.\frac{\partial n}{\partial p^j}\right|_{E[\mathbf{Z}]}\right)^2 \sigma_p^2 + \sum_{j=1}^{q}\left(\left.\frac{\partial n}{\partial t^j}\right|_{E[\mathbf{Z}]}\right)^2 \sigma_t^2 \\ &+ \sum_{j=1}^{q}\left(\left.\frac{\partial n}{\partial h^j}\right|_{E[\mathbf{Z}]}\right)^2 \sigma_h^2 + \left(\left.\frac{\partial n}{\partial \mu^j}\right|_{E[\mathbf{Z}]}\right)^2 \sigma_\mu^2 \end{aligned} \quad (28)$$

$$\begin{aligned} Var[R(\mathbf{Z})] &\equiv \sigma_R^2 \\ &= \left(\left.\frac{\partial R}{\partial r_0}\right|_{E[\mathbf{Z}]}\right)^2 \sigma_{r_0}^2 + \left(\left.\frac{\partial R}{\partial r_{45}}\right|_{E[\mathbf{Z}]}\right)^2 \sigma_{r_{45}}^2 \\ &+ \left(\left.\frac{\partial R}{\partial r_{90}}\right|_{E[\mathbf{Z}]}\right)^2 \sigma_{r_{90}}^2 \end{aligned} \quad (29)$$

Therefore, for probabilistic modeling of stress-based FLD in section 4, the above new random vector, which consists of K, n, and R along with mean values and variances from Eq. (24) to (29) is used instead of the random vector $\mathbf{Z} = [p^i, \cdots, p^q, t^i, \cdots, t^q, h^i, \cdots, h^q, \mu]^T$.

4. Probabilistic modeling of stress-based FLD

4.1 Limit state function

The possibility of bursting failure in metal forming processes can be usually estimated in practice by using strain-based FLD, in which major principal strain values are plotted against minor principal strain values. The deformation having strain distributions below the FLC is considered safe from necking or bursting. On the other hand, the region above the FLC is regarded as unsafe during the forming operation. Since the FLC usually approximates experimental results which exhibit unavoidable scatter, the FLD can be considered to have three kinds of zones such as safe, failed and marginal zone as shown in Fig. 1. In a similar manner, a safe zone of a stress-based FLD is considered as the region where failure is highly improbable, while the failed zone is regarded as the one defining stress states with a high probability of failure. In general, between the two zones, a marginal zone is introduced with the probability of failure high enough so that the stress state cannot be considered safe. Hence, the reliability of the stress-based FLD is defined as the probability of the limit

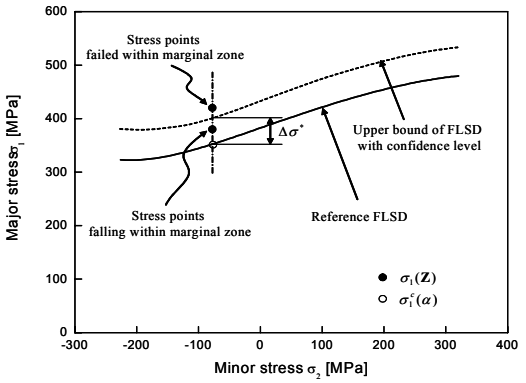

Fig. 3. Schematic representation of the size of permissible region.

stresses falling within the marginal zone with the specified permissible region. For a given stress ratio α, the definition of a limit state function $G(\mathbf{Z})$ that will be used in reliability analysis is as follows:

$$G(\mathbf{Z}) = \left(\sigma_1^c(\alpha) + \Delta\sigma^*\right) - \sigma_1(\mathbf{Z}) \tag{30}$$

where $\Delta\sigma^*$ is a the size of the permissible region which is usually a distance between a $\sigma_1^c(\alpha)$ and upper bound of a forming limit curve on the stress-based FLD as shown in Fig. 3. And $\sigma_1(\mathbf{Z})$ is an actual limit stress obtained from in Eq. (9), and $\mathbf{Z}$ is a random vector associated with material parameters, namely $\mathbf{Z} = [K, n, R]^T$ along with their corresponding mean values and variances. Therefore, the reliability of stress-based FLD, which is the probability of the limit stresses existing within the marginal zone, is represented as

$$\textit{Reliability} = 1 - \Pr[G(\mathbf{Z}) \le 0] = 1 - \int_{G(\mathbf{Z})\le 0} f_Z(\mathbf{Z}) d\mathbf{Z} \tag{31}$$

where $f_z(\mathbf{Z})$ is a marginal probability density function of $\mathbf{Z}$.

4.2 Eliability assessment using first-order reliability method

Since it is difficult not only to define the probability function but also to compute the probability in Eq. (31), the first-order reliability method(FORM) is adopted in this work. In FORM, the probability of the limit stress existing within the marginal zone can be represented by the minimum distance from the limit state function $G(\mathbf{Z}) = 0$ to the origin of the reduced variates [13]. The point on the failure surface, $(Z_1'^*, Z_2'^*, \cdots, Z_s'^*)$, having the minimum distance to the origin may be determined as

$$\begin{aligned} &\text{Minimize} \quad (\mathbf{Z}'^T\mathbf{Z}')^{1/2} \\ &\text{s.t} \qquad G(\mathbf{Z}) = 0 \end{aligned} \tag{32}$$

where the uncorrelated reduced variates are $Z_i' = (Z_i - \bar{Z}_i)/\sigma_{Z_i}$, where $\bar{Z}_i$ is a mean value and σ_{Z_i} is its standard deviation of random variable Z_i, respectively. Using the method of Lagrange's multiplier,

$$\mathbf{\Pi} = (\mathbf{Z}'^T\mathbf{Z}')^{1/2} + \lambda G(\mathbf{Z}) \tag{33}$$

To minimize $\mathbf{\Pi}$, the following conditions should be satisfied:

$$\frac{\partial \mathbf{\Pi}}{\partial \mathbf{Z}'} = \frac{\mathbf{Z}'}{(\mathbf{Z}'^T\mathbf{Z}')^{1/2}} + \lambda \frac{\partial G}{\partial \mathbf{Z}'} = 0 \tag{34}$$

$$\frac{\partial \mathbf{\Pi}}{\partial \lambda} = G(\mathbf{Z}) = 0 \tag{35}$$

where the gradient vectors are $\nabla\mathbf{G} = [\partial G/\partial Z_1', \partial G/\partial Z_2', \cdots, \partial G/\partial Z_s']^T$. From Eq. (35), $\lambda = (\nabla\mathbf{G}^T\nabla\mathbf{G})^{-1/2}$. Thus the minimum distance yields $(\mathbf{Z}'^T\mathbf{Z}')_{\min}^{1/2} = \omega$ as

$$\omega = \frac{-\nabla\mathbf{G}^{*T}\mathbf{Z}'^*}{(\nabla\mathbf{G}^{*T}\nabla\mathbf{G}^*)^{1/2}} \tag{36}$$

where the derivatives $\nabla\mathbf{G}^*$ are evaluated at $(Z_1'^*, Z_2'^*, \cdots, Z_s'^*)$. Using the reliability index ω, the most probable point on the failure surface becomes $Z_i'^* = -\gamma_i^*\omega$, in which γ_i^* is the direction cosines along the axes Z_i' are as follows:

$$\gamma_i^* = \frac{\left(\dfrac{\partial G}{\partial Z_i'}\right)_*}{\sqrt{\displaystyle\sum_{i=1}^{s}\left(\frac{\partial G}{\partial Z_i'}\right)_*^2}} \tag{37}$$

For a limit state function $G(\mathbf{Z})$, the first-order reliability method employed in this work can be summarized as the following six steps:

(a) Assume initial values of Z_i^*; i = 1, 2, … , s and obtain

$$Z_i'^{*} = \frac{Z_i^{*} - \bar{Z}_i}{\sigma_{Z_i}}$$

(b) Evaluate $(\partial G / \partial Z_i')_*$ and γ_i^* at $Z_i'^{*}$.
(c) Form $Z_i^{*} = \bar{Z}_i - \gamma_i^* \sigma_{Z_i} \omega$.
(d) Substituting above Z_i^{*} in $G(Z_1^{*}, Z_2^{*}, \ldots, Z_s^{*}) = 0$ and solve for ω.
(e) Using the ω obtained in Step (d), reevaluate $Z_i'^{*} = -\gamma_i^{*} \omega$.
(f) Repeat Steps (b) through (e) until convergence is obtained.

4.3 Monte-Carlo simulation

The reliability of stress-based FLD obtained from the analytical method using FORM is verified with the Monte-Carlo simulation(MCS). The raw random numbers generated by a computer, which follows a given probability distribution of the variable, are used to devise the strength coefficient, work hardening exponent and normal anisotropy values. The three random material parameters can be obtained as

$$\begin{aligned} K &= \bar{K} + r_1 \sigma_K \\ n &= \bar{n} + r_2 \sigma_n \\ R &= \bar{R} + r_3 \sigma_R \end{aligned} \tag{38}$$

where r_1, r_2 and r_3 are zero-mean random numbers obeying standard normal distribution law. From the Eq. (38), the process of generating random material parameters is repeated a number of sample times. Consequently the reliability of stress-based FLD using MCS is estimated by the ratio of the number of the stress points existing within the marginal zone to the total number of samples as below.

$$Reliability = \frac{Number\ of\ stress\ points\ existed\ within\ marginal\ zone}{Total\ number\ of\ samples} \tag{39}$$

To compare the reliabilities obtained from the analytical method and the simulation method, the accuracy of the computed reliability from the Monte-Carlo simulation should be estimated. Moreover, it is desirable to know how many simulations, i.e. sample size, are required to obtain a certain accuracy. By approximating the binominal distribution with a normal distribution, the following expression for the percent error has been developed [13]:

$$\%Error = 200 \sqrt{\frac{1 - \Pr[G(\mathbf{Z}) \le 0]}{Total\ number\ of\ samples \times \Pr[G(\mathbf{Z}) \le 0]}} \tag{40}$$

In this work, in order to confirm the accuracy of the estimated failure probability $\Pr[G(\mathbf{Z}) \le 0] = 0.0001 \pm 0.00002$, i.e. reliability of 0.9999 ± 0.00002, the total number of samples of 1,000,000 is used.

5. Results

5.1 Analytically determined standard deviations of K, n and R

Consider a tube with the initial inner radius of 32.5 mm, wall thickness of 2.0 mm and total length of 300 mm. Experimental data measured from a bulging test for the tube under five different pressure levels are listed in Table 1. All measured data were considered as normally distributed random variables. Since only five samples for each pressure level have been used, the standard deviation of each data was appropriately presumed. First, in order to evaluate the statistical correlation between the material parameters and measured data, the internal pressure *p*, thickness *t*, bulge height *h*, and friction coefficient μ were randomly generated by a computer. Since three anisotropy parameters r_0, r_{45} and r_{90} are unchangeable during the entire procedure of the bulging test, the anisotropy parameter was taken as deterministic $\bar{R}$ of

Table 1. Experimentally measured data and random variables.

Random variable	Internal pressure		Thickness	Bulge height	
	p [MPa]		t [mm]	h [mm]	
Mean value	1	17.08	1.980	65.90	
	2	18.00	1.958	66.20	
	3	18.97	1.924	66.75	
	4	19.98	1.892	68.15	
	5	20.08	1.668	77.70	
Standard deviation	σ_p		σ_t	σ_h	
Distribution type	Normal		Normal	Normal	
Random variable	Friction coefficient		Anisotropy parameters		
	μ		r_0	r_{45}	r_{90}
Mean value	0.1		1.43	0.87	1.54
Standard deviation	σ_μ		σ_{r_0}	$\sigma_{r_{45}}$	$\sigma_{r_{90}}$
Distribution type	Normal		Normal	Normal	Normal

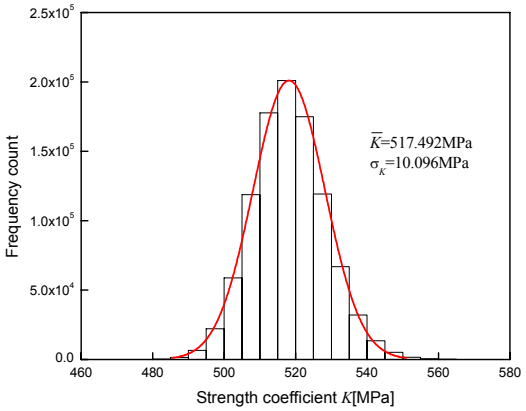

Fig. 4. Statistical histogram for strength coefficient K generated randomly with σ_p =0.1 MPa, σ_t =0.01 mm, σ_h =0.1 mm, σ_μ =0.01.

1.1775 during generating the measured data of the bulging test. Fig. 4 shows the statistical histogram for the strength coefficient K generated from 1,000,000 samples. The histograms for the work-hardening exponent n and the normal anisotropy value R are plotted in Figs. 5 and 6. Table 2 lists the comparison of mean values and standard deviations of K and n obtained analytically and statistically with the standard deviations of the measured data σ_p =0.1 MPa, σ_t =0.01 mm, σ_h =0.1 mm, σ_μ = 0.01, and $\bar{R}$ =1.1775. When there is enough data about experimental measurements of p, t and h, the standard deviations of the data can be statistically obtained. As mentioned above, since sufficient data is not available, those standard deviations were properly assumed in this study. In addition, the table compares the mean value and standard deviation of the anisotropy parameter R with the deviation of $\sigma_{r_0} = \sigma_{r_{45}} = \sigma_{r_{90}}$ =0.1. The errors between the analytical and the statistical results of the standard deviation are 0.63% for the strength coefficient K, 0.03% for the work-hardening exponent n, and 0.02% for the anisotropy value R in the given variations of measured data. As listed in the table, the standard deviations of the material parameters can be successfully predicted from Eqs. (25), (28) and (29). Thus, it is validated that the variation of the new random variables K, n, R, which are actually random outputs of measured data listed in Table 1, can be substituted for directly by utilizing the measured data to assess the reliability of the stress-based FLD. The nominal stress-based FLD obtained with the mean values of the material parameters listed in Table 2 is plotted as a "reference FLSD" in Fig. 3.

Table 2. Mean values and standard deviations of material parameters obtained stochastically and analytically.

Material parameters		Statistical result(I)	Statistical result(II)	Analytical result	Error [%]
K [MPa]	$\bar{K}$	517.503	517.492	515.967	0.30
	σ_K	10.076	10.096	10.150	0.63
n	$\bar{n}$	0.1697	0.1697	0.1675	1.30
	σ_n	7.7579E-3	7.7721E-3	7.7626E-3	0.03
R	$\bar{R}$	1.1774	1.1775	1.1775	0.00
	σ_R	6.1141E-2	6.1310E-2	6.1237E-2	0.02

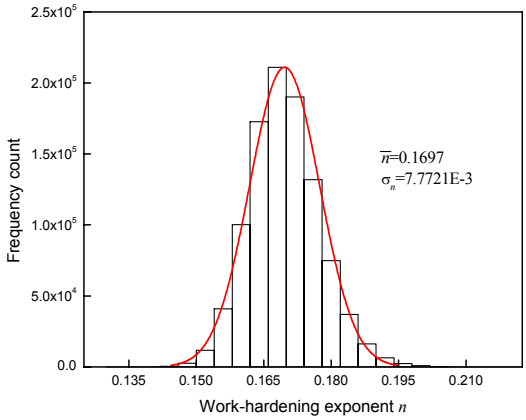

Fig. 5. Statistical histogram for work-hardening exponent n generated randomly with σ_p =0.1 MPa, σ_t =0.01 mm, σ_h =0.1 mm, σ_μ =0.01.

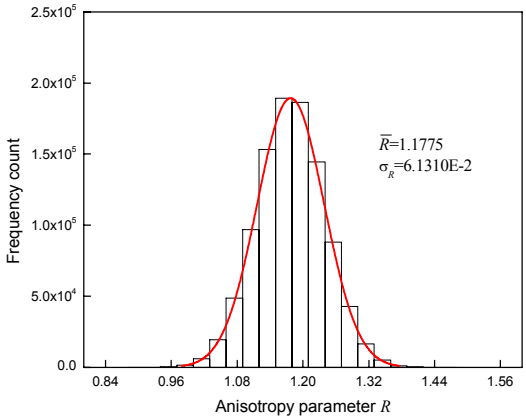

Fig. 6. Statistical histogram for anisotropy parameter R generated randomly with $\sigma_{r_0} = \sigma_{r_{45}} = \sigma_{r_{90}}$ =0.1.

Moreover, in order to compare the stress-based FLD in Fig. 3 and a strain-based FLD in the tube hydroforming process, the nominal strain-based FLD calculated with the same material parameters listed in Table 2 is shown in Fig. 7.

Table 3. Probability of limit stresses existing within marginal zone with different sizes of permissible region(σ_K =10.150 MPa, σ_n =7.7626E-3, σ_R =6.1237E-2, α =0.5).

$\Delta\sigma^*$ [MPa]	FORM	MCS(I)	MCS(II)	Error (%)
0	0.50000	0.49803	0.49791	0.41
5	0.71748	0.71346	0.71315	0.59
10	0.87371	0.86800	0.86799	0.66
15	0.95587	0.95209	0.95188	0.41
20	0.98798	0.98660	0.98619	0.16
25	0.99744	0.99691	0.99687	0.06
30	0.99957	0.99947	0.99944	0.01

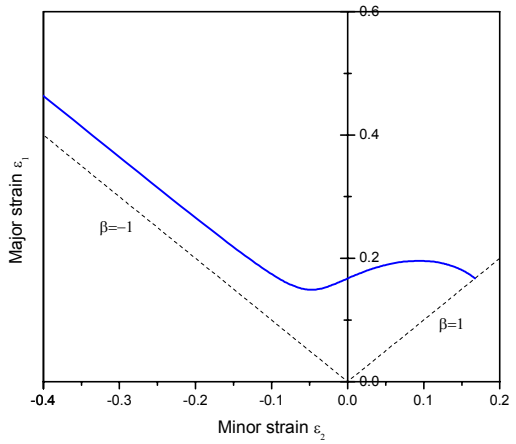

Fig. 7. Nominal strain-based FLD calculated with $\bar{K}$ = 515.967 MPa, $\bar{n}$ =0.1675, and $\bar{R}$ =1.1775.

5.2 Reliability assessment using FORM

To analytically calculate the probability of limit stresses existing within the marginal zone in Eq. (31), the first-order reliability method(FORM) is adopted and verified with Monte-Carlo simulation(MCS). As a result, Table 3 compares the probabilities calculated from FORM and MCS with different size of permissible region taking the standard deviation of the three material parameters as σ_K =10.150 MPa, σ_n = 7.7626E-3, σ_R =6.1237E-2 under the stress ratio α =0.5. These standard deviations come from the standard deviations of the measured data σ_p =0.1 MPa, σ_t =0.01 mm, σ_h =0.1 mm, σ_μ = 0.01, and $\sigma_{r_0} = \sigma_{r_{45}} = \sigma_{r_{90}}$ =0.1. The simulation usually takes about 2.82 seconds on a Compaq Alpha-EV6.7 CPU(667 MHz), while the analytical method takes about 1.95 milliseconds on the same machine. It is evident that the probability of limit stresses falling within the marginal zone is increased with increasing the permissible region of the marginal zone. The maximum error between the analytical and the simulation method is 0.66% in the given variation of material parameters. From the results, it is verified that the reliability of stress-based FLD, which is defined as the probability of limit stresses falling within the marginal zone, can be successfully calculated based on FORM.

Table 4. Probability of limit stresses existing within marginal zone with respect to deviation of bulge test data($\Delta\sigma^*$ = 20 MPa, σ_R =6.1237E-2, α =0.5)

Standard deviation of bulge test data		Standard deviation of material parameters		Probability
		σ_K [MPa]	σ_n	
σ_p [MPa]	0.01	9.262	7.325E-3	0.9926
	0.1	10.150	7.763E-3	0.9880
	0.2	12.459	8.960E-3	0.9704
	0.5	22.820	1.485E-2	0.8574
σ_t [mm]	0.001	6.668	4.640E-3	0.9992
	0.01	10.150	7.763E-3	0.9880
	0.02	16.746	1.333E-2	0.9224
	0.05	39.018	3.161E-2	0.7326
σ_h [mm]	0.01	9.058	6.835E-3	0.9936
	0.1	10.150	7.763E-3	0.9880
	0.2	12.906	1.006E-3	0.9654
	0.5	24.727	1.971E-2	0.8352
σ_μ	0.001	9.889	7.713E-3	0.9894
	0.01	10.150	7.763E-3	0.9880
	0.05	15.158	8.889E-3	0.9441
	0.1	25.017	1.173E-2	0.8389

5.3 Statistical evaluation of stress-based FLD

The reliability for limit stresses existing within the marginal zone, whose band width is assumed to be $\Delta\sigma^*$ =20 MPa under the stress ratio α =0.5, with respect to the standard deviation of the measured data obtained from a bulge test is given in Table 4. As can be seen, the reliabilities are decreased with increasing the standard deviation of the measured data. Table 5 lists probabilities of limit stresses existing within the marginal zone with respect to different deviation of anisotropy parameters taking the size of permissible region and the standard deviation of the other parameters as $\Delta\sigma^*$ =20 MPa, σ_K =10.150 MPa, σ_n = 7.763E-3. It leads to decrease of the probability with increasing the standard deviation of the anisotropy parameters.

To statistically evaluate the forming limit on the stress-based FLD, three example cases with different standard deviations of random variables were employed as listed in Table 6. Using the three different

Table 5. Probability of limit stresses existing within marginal zone with respect to deviation of anisotropy parameters($\Delta\sigma^*$ =20 MPa, σ_K =10.150 MPa, σ_n =7.763E-3, α = 0.5).

Standard deviation of anisotropy parameters		σ_R	Probability
σ_{r_0} $\sigma_{r_{90}}$	0.01	5.596E-2	0.9887
	0.1	6.124E-2	0.9880
	0.2	7.500E-2	0.9857
	0.5	1.369E-1	0.9655
$\sigma_{r_{45}}$	0.01	3.571E-2	0.9906
	0.1	6.124E-2	0.9880
	0.2	1.061E-1	0.9777
	0.5	2.525E-1	0.8948

Table 6. Standard deviations of random variables for case study.

Variable	Unit	Case I	Case II	Case III
σ_p	MPa	0.1	0.25	0.5
σ_t	mm	0.01	0.025	0.05
σ_h	mm	0.1	0.25	0.5
σ_μ	-	0.01	0.025	0.1
σ_{r_0}	-	0.1	0.15	0.2
$\sigma_{r_{45}}$	-	0.1	0.15	0.2
$\sigma_{r_{90}}$	-	0.1	0.15	0.2
σ_K	MPa	10.150	25.374	54.511
σ_n	-	7.763E-3	1.941E-2	3.956E-2
σ_R	-	6.124E-2	9.186E-2	1.225E-1

Table 7. Band width of FLSD with desired confidence level.

Confidence Level	β	α	$\Delta\sigma^*$ [MPa]		
			Case I	Case II	Case III
75%	-0.75	-0.352	4.897	12.402	26.736
	-0.50	0.056	5.042	13.109	28.546
	0.00	0.541	6.052	14.539	30.885
	0.10	0.614	6.448	15.196	32.092
	0.20	0.668	6.948	16.086	33.832
90%	-0.75	-0.352	9.309	23.586	50.792
	-0.50	0.056	9.601	25.033	54.832
	0.00	0.541	11.581	27.930	59.788
	0.10	0.614	12.364	29.276	62.465
	0.20	0.668	13.350	31.130	66.488
99%	-0.75	-0.352	16.939	42.901	92.371
	-0.50	0.056	17.530	45.967	102.267
	0.00	0.541	21.333	51.838	113.131
	0.10	0.614	22.841	54.651	119.715
	0.20	0.668	24.767	58.668	130.791

standard deviations of the measured data, the band width of marginal zone to be able to satisfy the desired confidence level was determined and listed in Table 7. At the given deviations as σ_p =0.1 MPa, σ_t =0.01 mm, σ_h =0.1 mm, σ_μ =0.01 and $\sigma_{r_0} = \sigma_{r_{45}} = \sigma_{r_{90}}$ =0.1, the size of the permissible region at plane strain path, i.e. $\beta = 0$ or $\alpha = 0.541$, is

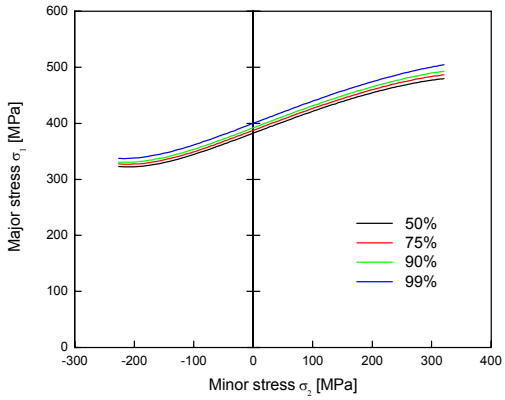

Fig. 8. Forming limit stress diagrams for Case I along with different confidence levels.

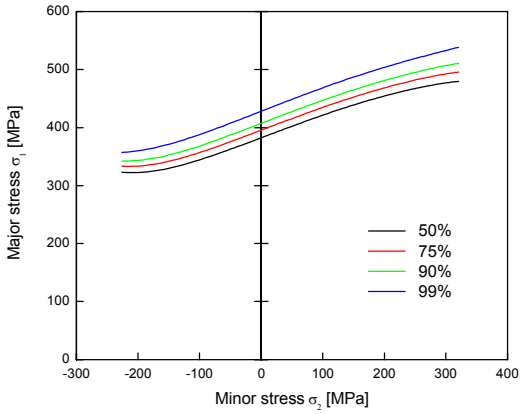

Fig. 9. Forming limit stress diagrams for Case II along with different confidence levels.

increased from 6.052 MPa up to 21.333 MPa with increasing confidence level from 75% to 99%. In the case of σ_p =0.5 MPa, σ_t =0.05 mm, σ_h =0.5 mm, σ_μ =0.05, and $\sigma_{r_0} = \sigma_{r_{45}} = \sigma_{r_{90}}$ =0.2, the band width of the stress-based FLD should be increased from 30.885 MPa to 113.131 MPa to satisfy their corresponding confidence level from 75% to 99%. As can be seen, the larger deviation of the measured data results in the wider marginal zone on the locus of the FLC at the same confidence level. In addition, the increased stress ratio brings out the broader band width of the FLC as well. Figs 8, 9 and 10 show the upper bound of the stress-based FLD to be satisfied with a confidence level of 50%, 75%, 90% and 99% at the given material parameter deviations. It is well noted that a smaller deviation of material parameter results in narrower band width of the forming limit curve on the stress-based FLD.

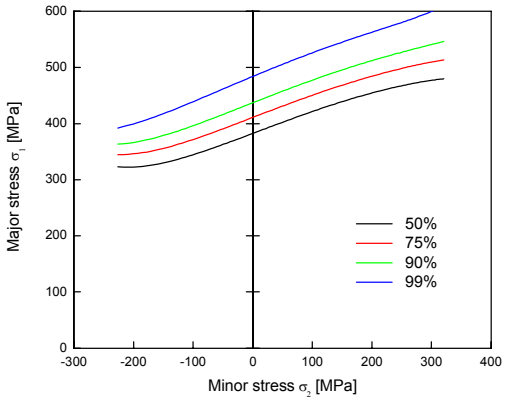

Fig. 10. Forming limit stress diagrams for Case III along with different confidence levels.

6. Conclusions

In this work, with taking into account the random characteristics throughout the experiment procedure, a novel approach to statistically predicting a bursting failure in hydroforming processes was proposed. Since bursting is an irrecoverable phenomenon due to local instability, the analytical stress-based FLD using the classical diffuse necking criterion was introduced. In order for stochastic modeling of the stress-based FLD with confidence level, all experimental data measured during a bulge test are assumed as normally distributed random variables. And then the statistical correlation between the measured data during the bulge test and the material parameters was evaluated by using the first-order approximated mean value and variance. The errors between the analytically predicted standard deviation and the statistical results are 0.63% for the strength coefficient *K,* 0.03% for the work-hardening exponent *n*, and 0.02% for the anisotropy value *R* in the given variations of measured data. In addition, in order to assess the reliability of stress-based forming limit curve, a first-order reliability method was adopted and verified with Monte-Carlo simulation method. As a result, the errors between the analytical and the simulation method were less than 0.66% in the given variation of material parameters. It is implied that the reliability of stress-based FLD, which is defined as the probability of limit stresses falling within the marginal zone, can be successfully calculated based on the first-order reliability method. Moreover, at a given deviation of material parameters, the bandwidth of the forming limit curve on the stress-based FLD was increased with increasing confidence level. A larger deviation of the material parameters results in a wider marginal zone on the locus of the FLC at the same confidence level. The increased stress ratio brings out a little broader band width of the FLC as well. With the proposed approach, a product designer and manufacturing engineer can be helped to robustly evaluate the forming limit in hydroforming processes.

Acknowledgment

This work was supported by the Korea Research Foundation Grant funded by the Korean Government (MOEHRD, Basic Research Promotion Fund) (KRF-2008-331-D00034). Also the last author would like to express his thanks for the support of the Korea Science and Engineering Foundation (KOSEF) NRL Program grant funded by the Korea government (MEST) (No. R0A-2008-000-2 0017-0), and the partial support by grants-in-aid for the National Core Research Center Program from MOST/KOSEF (No. R15-2006-022-02002-0).

References

[1] H. J. Kleemola and M. T. Pelkkikangas, Effect of predeformation and strain path on the forming limits of steel, copper and brass, *Sheet Metal Industries*, 63 (1977) 591-599.

[2] T. B. Stoughton, A general forming limit criterion for sheet metal forming, *Int. J. Mech. Sci.*, 42 (1999) 1-27.

[3] T. B. Stoughton and X. Zhu, Review of theoretical models of the strain-based FLD and their relevance to the stress-based FLD, *Int. J. Plast.*, 20 (2004) 1463-1486.

[4] M. C. Butuc, J. J. Gracio and B. D. Rocha, An experimental and theoretical analysis on the application of stress-based forming limit criterion, *Int. J. Mech. Sci.*, 48 (2006) 414-429.

[5] CHM. Simha, J. Gholipour, A. Bardelcik and M. J. Worswick, Prediction of Necking in Tubular Hydroforming Using an Extended Stress-Based Forming Limit Curve, *J. Eng. Mater. Technol.*, 129 (2007) 36-47.

[6] D. Banabic and M. Vos, Modelling of the Forming Limit Band–A new Method to Increase the Robustness in the Simulation of Sheet Metal Forming Processes, *CIRP Annals – Manuf. Technol.*, 56 (2007) 249-252.

[7] M. Strano M and B. M. Colosimo, Logistic regression analysis for experimental determination of

forming limit diagrams, *Intl. J. Mach. Tools Manuf.*, 46 (2006) 673-682.
[8] K. Janssens, F. Lambert and S. Vanrostenberghe, Vermeulen M Statistical evaluation of the uncertainty of experimentally characterised forming limits of sheet steel, *J. Mater. Process. Technol.*, 112 (2001) 174-184.
[9] M. Kleiber, J. Rojek and R. Stocki, Reliability assessment for sheet metal forming operations. *Comput. Methods Appl. Mech. Engrg.*, 191 (2002) 4511-4532.
[10] R. Hill, *The Mathematical Theory of Plasticity*. Oxford University Press, Oxford, UK, (1983).
[11] J. Kim, S. W. Kim, H. J. Park and B. S. Kang, A prediction of bursting failure in tube hydroforming process based on plastic instability, *Int. J. Adv. Manuf. Technol.*, 27 (2006) 518-524.
[12] W. J. Song, J. Kim and B. S. Kang, Experimental and analytical evaluation on flow stress of tubular material for tube hydroforming simulation, *J. Mater. Process. Technol.*, 191 (2007) 368-71.
[13] A. H. Ang and W. H. Tang, *Probability concepts in Engineering Planning and Design I, II*. John Wiley & Sons Press, New York, USA, (1984).

Jeong Kim received his B.S. in Mechanical Design Engineering from Pusan National University, Korea, in 1989. He then received his M.S. in Mechanical Engineering from Korea Advanced Institute of Science and Technology, and Ph.D. in Aerospace Engineering from Pusan National University in 1991 and 2002, respectively. Dr. Kim is currently an Associate Professor at the Department of Aerospace Engineering at Pusan National University in Busan, Korea. His research interests include aircraft optimal design and structure analysis with FEM.

Beom-Soo Kang received his B.S. in Mechanical Engineering Pusan National University, Korea, in 1981. He then received his M.S. in Aerospace Engineering from Korea Advanced Institute of Science and Technology, and Ph.D. in Mechanical Engineering from University of California at Berkeley, USA, in 1983 and 1990, respectively. Dr. Kang is currently a Professor at Department of Aerospace Engineering and ERC/NSDM at Pusan National University in Busan, Korea. His research interests include CAE of manufacturing processes, stress analysis by FEM, and UAV(Unmanned Aerial Vehicle) system.